Available online at www.sciencedirect.com
SCIENCE DIRECT®
International Journal of Heat and Mass Transfer 48 (2005) 4446–4459
International Journal of HEAT and MASS TRANSFER
www.elsevier.com/locate/ijhmt

On the rise paths of single vapor bubbles after the departure from nucleation sites in subcooled upflow boiling

Tomio Okawa [a,*], Tatsuhiro Ishida [a], Isao Kataoka [a], Michitsugu Mori [b]

[a] Department of Mechanophysics Engineering, Osaka University, 2-1, Yamadaoka, Suita-shi, Osaka 565-0871, Japan
[b] Nuclear Power R&D Center, Tokyo Electric Power Company, 4-1, Egasaki-cho, Tsurumi-ku, Yokohama 230-8510, Japan

Received 15 April 2003; received in revised form 22 April 2005

Abstract

A photographic study was carried out for the subcooled flow boiling of water to elucidate the rise characteristics of single vapor bubbles after the departure from nucleation sites. The test section was a transparent glass tube of 20 mm in inside diameter and the flow direction was vertical upward; liquid subcooling was parametrically changed within 0–16 K keeping system pressure and liquid velocity at 120 kPa and 1 m/s, respectively. The bubble rise paths were analyzed from the video images that were obtained at the heat flux slightly higher than the minimum heat flux for the onset of nucleate boiling. In the present experiments, all the bubbles departed from their nucleation sites immediately after the inception. In low subcooling experiments, bubbles slid upward and consequently were not detached from the vertical heated wall; the bubble size was increased monotonously with time in this case. In moderate and high subcooling experiments, bubbles were detached from the wall after sliding for several millimeters and migrated towards the subcooled bulk liquid. The bubbles then reversed the direction of lateral migration and were reattached to the wall at moderate subcooling while they collapsed due to the condensation at high subcooling. It was hence considered that the mechanisms of the heat transfer from heated wall and the axial growth of vapor volume were influenced by the difference in bubble rise path. It was observed after the inception that bubbles were varied from flattened to more rounded shape. This observation suggested that the bubble detachment is mainly caused by the change in bubble shape due to the surface tension force.

Keywords: Subcooled flow boiling; Photographic study; Bubble; Detachment; Rise path

1. Introduction

Vertical upward subcooled flow boiling of water is frequently encountered in various industrial applications. In nuclear power plants, in particular, important parameters including the reactor power and the inception of two-phase instability are influenced by the vapor volume in the subcooled boiling region. Thus, sufficient understanding of subcooled flow boiling is of considerable interest to improve the safety and performance of nuclear reactors.

In the flow of subcooled liquid in a heated channel, wall temperature increases gradually with the distance from the inlet. Heterogeneous bubble nucleation occurs at small cavities when the temperature near the heated

* Corresponding author. Tel.: +81 6 6879 7257; fax: +81 6 6879 7247.
E-mail address: t-okawa@mech.eng.osaka-u.ac.jp (T. Okawa).

0017-9310/$ - see front matter © 2005 Elsevier Ltd. All rights reserved.
doi:10.1016/j.ijheatmasstransfer.2005.05.026

Nomenclature

D	tube diameter (m)
d_b	bubble size (m)
$d_{b,max}$	maximum bubble size (m)
k	thermal conductivity (W/mK)
N	number of activated nucleation sites
P	pressure (Pa)
Pr	Prandtl number
q	heat flux (W/m^2)
r	radius (m)
R	gas constant (m^2/s^2 K)
R_A	modified aspect ratio
Re	Reynolds number
T	temperature (K)
t_b	total time of a bubble cycle (ms)

Greek symbols

β	contact angle (radian)
λ	latent heat of vaporization (J/kg)
ρ	density (kg/m^3)
σ	surface tension (N/m)

Subscripts

0	2.5 ms after the nucleation
c	cavity
g	gas
l	liquid
r	radial
onb	onset of nucleate boiling
sat	saturation
sub	subcooling
w	wall
z	axial
θ	circumferential

surface is high enough. The inception of vapor bubbles is known as the onset of nucleate boiling (ONB). After ONB, the heat transfer rate from the wall is increased but total vapor volume can remain low and fairly constant. At certain distance from the point of ONB, a rapid increase of vapor volume is initiated though the temperature of bulk liquid is still below the saturation temperature. This location is referred to the point of net vapor generation (NVG) or the onset of significant void (OSV). The prediction of the point of NVG is one of the critical problems in the subcooled flow boiling particularly from the standpoint of the vapor void fraction in the heated channel. There exist several empirical correlations for the point of NVG [1,2]. Though these correlations provide good predictions in many conditions of practical interest, several researchers reported severe limitations of the models in some thermal hydraulic conditions [3–5]. Since the wall is superheated but the temperature of bulk liquid is below the saturation temperature in subcooled flow boiling, vapor bubbles generated at nucleation sites may be condensed more rapidly if they are detached from the heated wall. This leads to the decrease of vapor volume in the channel cross-section. It is hence considered that the experimental information on the behavior of vapor bubbles is of significant importance to develop the improved mechanistic model for the forced convective subcooled flow boiling.

Visual observations of vapor bubbles in vertical upflow boiling were conducted by many researchers for subcooled liquids [6–14] and for saturated or slightly subcooled liquids [15–18]. In the subcooled flow boiling, bubble population is low and consequently the influence from neighboring bubbles may be negligible at low heat flux while the interaction and coalescence of bubbles complicates significantly the phenomena at high heat flux. However, despite the extensive photographic studies, the bubble behavior in forced convective boiling has not been thoroughly understood even in the low bubble population condition. Thorncroft et al. [17] concluded from their experimental data for refrigerant FC-87 that typical bubbles in vertical upflow boiling slide upward the heated wall after the departure from nucleation sites and are not detached from the wall. Several other observations [6,8,15] may support this conclusion. On the other hand, Bibeau and Salcudean [12], Prodanovic et al. [14], van Helden et al. [16] and Okawa et al. [18] observed that the vapor bubbles generated at nucleation sites were detached from the vertical wall and migrated towards the bulk liquid. In the experiments by Okawa et al. for slightly subcooled water in a round tube [18], the detached bubbles reversed the direction of lateral migration and were then reattached to the wall; bubbles exhibited rebounding motion after the reattachment. In the experiments by Bibeau and Salcudean for highly subcooled water in an annular channel [12], bubbles collapsed due to condensation after the detachment.

The literature review for the photographic study on the subcooled upflow boiling in vertical channels indicated that the two distinct rise paths might be possible for a bubble after the departure from a nucleation site: one is the sliding along a vertical surface and the other is the detachment from a heated wall. It would be obvious that the growth rate of a bubble is affected significantly by the difference in rise path since the bubble cannot receive the heat from the wall directly if it is

detached from the wall. However, the important parameters and mechanisms for the bubble rise path were not elucidated. In view of this, a visual experimental study of subcooled upflow boiling is conducted in the present work in order to investigate the mechanism of bubble detachment from a vertical heated wall.

2. Description of the experiments

The experimental apparatus used in this work is shown schematically in Fig. 1. Filtrated and deionized tap water is used as a working fluid. The water is circulated by a pump. The ultrasonic flow meter that is accurate within ±0.5% is used to measure the volumetric flowrate. The 15 kW plug heater is used to heat up and then keep the water temperature. After exiting the pre-heating section, the water enters the vertical tube of 20.0 mm in inside diameter. This section consists of the two long stainless steel tubes and the short transparent glass tube between them. The glass tube is used as a test section in the experiments. The top of these tubes is connected with the header tank open to atmosphere to separate vapor bubbles from continuous liquid phase. The fluid temperature is measured at the inlet and outlet of pre-heating section and at the two radial locations (center and extremity in the cross-section) at the outlet of test section with type-K thermocouples that are accurate within ±1.5 K. The pressure at the test section is measured with the pressure transducer that is accurate within ±0.5 kPa. An analog-to-digital converter attached to a personal computer records the measurements of flowrate, temperatures and pressure every one second. To determine the test condition, 30 samples per channel are averaged. In all the experimental conditions tested, the deviations of measured instantaneous liquid volumetric flux, fluid temperatures and pressure from the averaged ones were within 0.033 m/s, 0.95 K and 5.7 kPa, respectively.

Shown in Fig. 2 is a schematic of transparent test section. The test section is the 160.0 mm long sapphire glass tube; its inner and outer diameters are 20.0 and 23.0 mm, respectively. Sapphire glass was chosen as

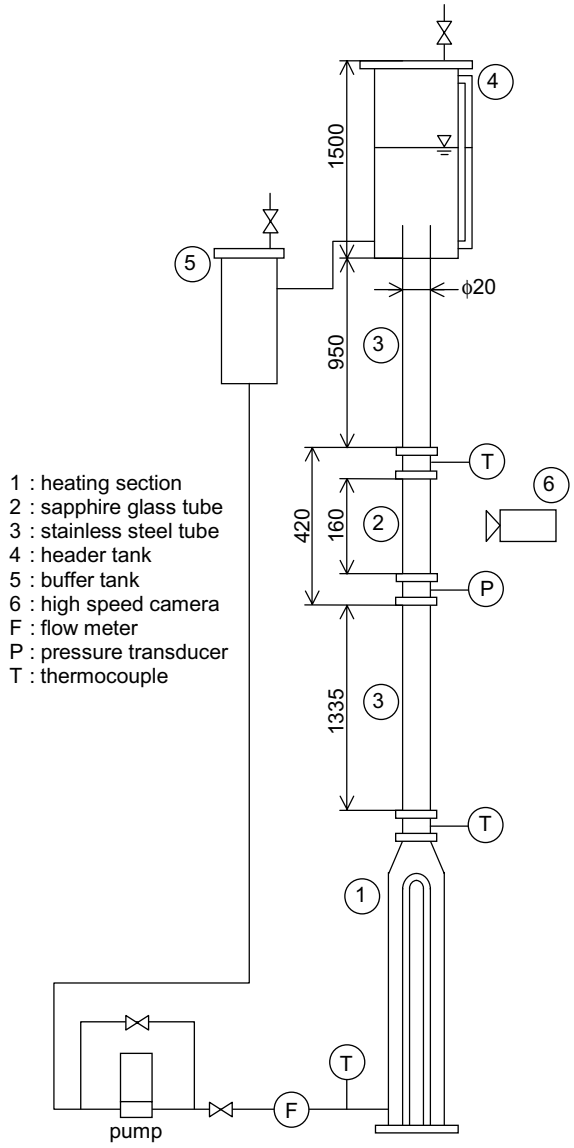

Fig. 1. Schematic diagram of the experimental apparatus.

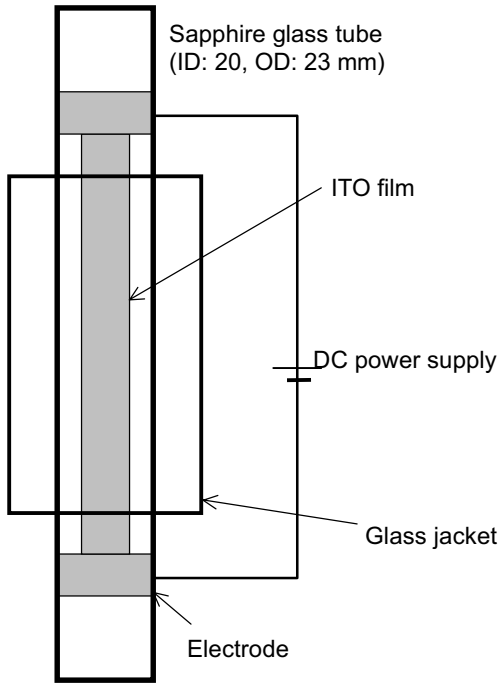

Fig. 2. Schematic diagram of the transparent test section.

the material for its higher thermal conductivity (46 W/mK at 300 K). The region of 12.2 mm in width and 100.0 mm in length on the outer surface of glass tube is coated with the thin indium tin oxide (ITO) film. The film thickness is estimated 0.2 μm; the ITO film does not deteriorate the transparency of glass tube significantly. Both ends of the ITO coated section are covered with nickel films, that are used as electrodes. The resistance of ITO film is 300–330 Ω depending on temperature and it is electrically heated with 5 kW DC power supply to generate vapor bubbles on the inner surface of the test section. A digital multimeter measures the voltage and the electric current with the uncertainties of ±0.1 V and ±2.3 mA, respectively. The uncertainty in the heat supplied to the test section is less than ±0.5%. In the present experiments, however, the test section is not thermally insulated for visual observation. The heat loss to ambient air is estimated to within 10%.

The successive bubble images are obtained with the two high-speed digital video cameras. The arrangement of cameras and illuminating lights is schematically shown in Fig. 3. To reduce the effect of refraction in bubble images, the glass tube is surrounded by a rectangular glass jacket and the gap between the tube and jacket is filled with silicone oil. The effect of refraction still remaining is corrected from the images of a specially designed acrylic piece inserted in the test section [18]. Digital video images of 512 × 256 pixels are recorded every 0.5 ms; the spatial resolution is approximately 0.1 mm and shutter speed is set at 0.125 ms.

Prior to the boiling experiments, the radial velocity profiles of single-phase liquid flow in the test section were measured using spherical polyester particles as tracers. The diameter and specific gravity of a particle were 0.2–0.4 mm and 1.04, respectively. In the single-phase experiments, the volumetric flux and temperature of liquid were varied within 0.5–2.0 m/s and 30–37 °C, respectively. The measured radial distributions of axial time-averaged liquid velocity agreed with the expression by Nunner for single-phase turbulent flow [19] within ±5%. The tracer particles were removed from the test loop using a filter for the experiments of flow boiling.

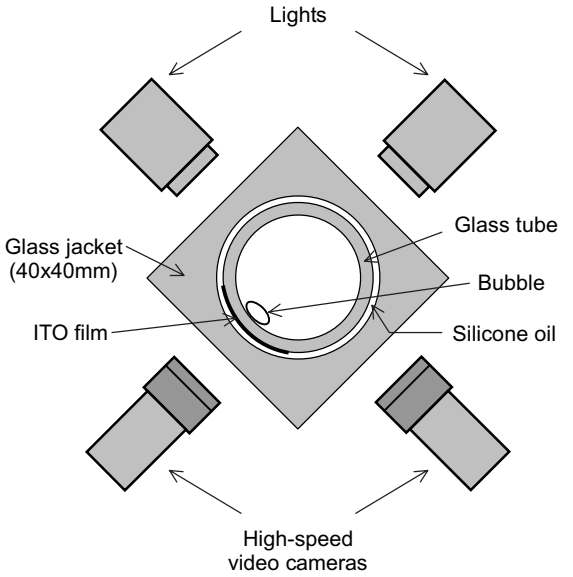

Fig. 3. Arrangement of high speed cameras and illuminating lights.

In the visualization tests of vapor bubbles, flowrate and temperature of liquid phase are controlled by adjusting the flow control valves and the power applied to the pre-heater, respectively. After steady state is established, DC power is supplied to the ITO film coated on the outer surface of test section tube. Parametrically changing the fluid temperature and applied heat flux, the side views and bottom views of vapor bubbles are recorded with the two synchronized high speed video cameras (see Fig. 3).

3. Results and discussion

3.1. Experimental conditions

The bubble behavior in the test section was recorded with the high speed video cameras in the twenty experimental conditions listed in Table 1. The locations of activated nucleation sites in the present experiments are depicted in Fig. 4. In Table 1, N denotes the locations of nucleation sites or the number of nucleation sites that were activated in each experimental condition, t_b is the averaged total time of a bubble cycle (sum of growth time and waiting time) and $d_{b,max}$ is the size of largest bubble observed in the test section. Here, t_b was measured for the bubbles generated at the nucleation site A is shown in Fig. 4. In all the boiling experiments reported in this work, the time-averaged test section pressure P and liquid phase volumetric flux U were within 118–124 kPa and 0.95–1.06 m/s, respectively. The heat fluxes applied to the ITO film q are plotted against the subcooling of bulk liquid T_{sub} in Fig. 5. Here, T_{sub} was deduced from the fluid temperature measured at the center at the outlet of glass tube. The flow patterns observed in the test section tube are also shown in the figure, which will be discussed in the following section.

In Fig. 6, the minimum heat fluxes required for the onset of nucleate boiling are compared with the following correlation by Davis and Anderson [20]:

$$(T_w - T_{sat})_{onb} = \frac{RT_{sat}^2 \ln[1 + 2\sigma B/r_c P]}{\lambda - RT_{sat} \ln[1 + 2\sigma B/r_c P]} + \frac{q_{onb} r_c}{k_l} \quad (1)$$

where B equals $(1 + \cos\beta)$ and the contact angle β is assumed $\pi/4$; if a sufficiently wide range of active cavity

Table 1
Summary of experimental data

Case	P (kPa)	U (m/s)	T_{sub} (K)	q (kW/m^2)	Flow pattern[a]	N[b]	t_b[c] (ms)	$d_{b,max}$ (mm)
A1	120	1.02	0.6	128	S	–	–	3.4
A2	119	0.99	0.0	182	S	B	–	4.3
B1	122	0.96	2.7	175	S/B	A	68.4	3.8
B2	121	0.96	2.4	213	S/B	A	11.2	3.6
B3	121	1.00	2.2	229	S/B	A–D	8.8	3.5
B4	121	0.95	2.4	246	S/B	A	8.4	4.3
B5	121	1.00	1.6	335	M	8	–	5.6
B6	120	1.01	1.4	460	M	–	–	9.7
C1	120	1.04	4.4	205	B/C	A	10.4	2.1
C2	123	1.02	4.8	228	B/C	A, B, E	6.4	1.9
C3	124	1.03	5.4	271	B/C	5	4.4	2.6
C4	120	1.00	4.4	355	M	7	3.3	5.5
C5	120	1.00	4.0	464	M	10	–	7.6
D1	119	1.02	8.1	337	C	5	4.8	3.7
D2	119	1.06	8.1	479	MC	6	2.0	4.3
D3	119	0.98	6.6	582	M	–	–	6.3
E1	121	1.03	15.6	290	C	6	3.4	0.9
E2	121	1.03	15.3	476	C	18	1.4	1.9
E3	121	1.04	15.0	597	MC	–	–	3.6
E4	118	1.02	14.0	717	MC	–	–	4.6

[a] S: sliding, B: bouncing, C: collapsing, M: merging, MC: merging then collapsing.
[b] Locations of nucleation sites are found in Fig. 4.
[c] Measured for the bubbles generated at the nucleation site A.

sizes is available on the heated surface, the modified critical cavity radius r_c is calculated by

$$r_c = \frac{B\sigma}{P} + \sqrt{\left(\frac{B\sigma}{P}\right)^2 + \frac{2Bk_l\sigma T_{sat}}{\lambda\rho_g q_{onb}}} \quad (2)$$

If r_c calculated from Eq. (2) is larger than the maximum active cavity size available on the heating surface, an estimate of the largest cavity size must be used for r_c. To estimate the wall temperature T_w, the following heat transfer equation is used:

$$q = 0.023 Re_l^{0.8} Pr_l^{0.4} \frac{k_l}{D}(T_w - T_{sub}) \quad (3)$$

Fig. 6 indicates that the calculated heat fluxes for ONB agree with the present experimental data if r_c is assumed 2 μm. From the comparisons with experimental data obtained under some engineering conditions using normal metal heater surface, Davis and Anderson [20] concluded that the size of cavities activated at ONB might be of the order of 1 μm. It is hence considered that the cavity size on the present glass surface is not different significantly from that on normal metal surface.

3.2. Observed flow patterns in the test section

The bubble behaviors observed in the test section tube are classified into five patterns as shown in Fig. 5. First, the snapshots from the side and bottom of heated surface at different heat fluxes are depicted in Fig. 7(a) and (b), respectively, in order to describe the effect of heat flux. The bulk liquid is slightly subcooled in these photographs ($T_{sub} = 1.4$–2.7 K). At low heat fluxes (175–246 kW/m^2), a small number of nucleation sites are activated. Although vapor bubbles depart from their nucleation sites immediately after the inception, the number density of vapor bubbles is low and bubble coalescence occurs very occasionally. As the heat flux is raised (335–460 kW/m^2), the number of activated nucleation sites and bubble population increase. A typical bubble merges with other bubbles that are generated at different nucleation sites. Also, some newly activated nucleation sites generate larger bubbles with lower frequency [23]. Thus, the size of largest bubble in the test section increases with the heat flux due to the increase in the number of activated nucleation sites and the occurrence of bubble coalescence. When the liquid subcooling is less than approximately 10 K, large bubbles repeated the coalescence with other bubbles at sufficiently high heat flux; thus, their volumes are increased gradually or become fairly constant while they move in the test section tube (the region of merging in Fig. 5). At higher subcooling, on the other hand, bubble coalescence also occurs frequently at sufficiently high heat flux; however, as depicted in Fig. 8, the volume of coalesced bubble is

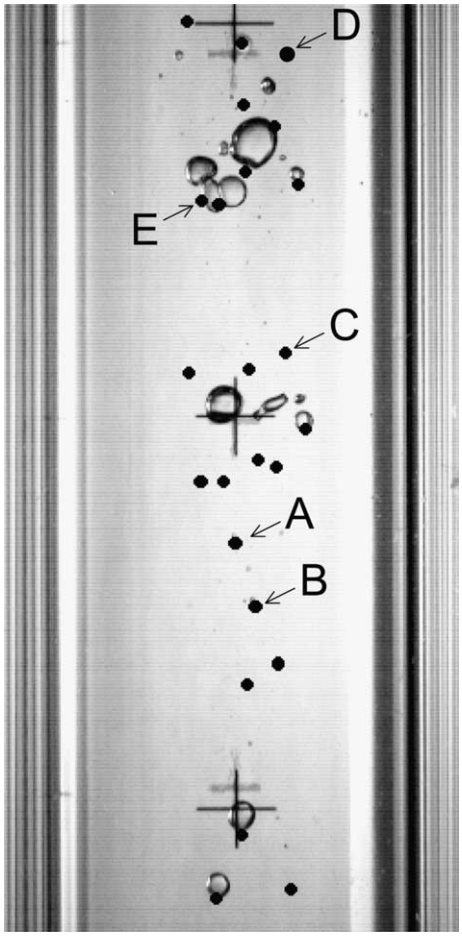

Fig. 4. Location of activated nucleation sites.

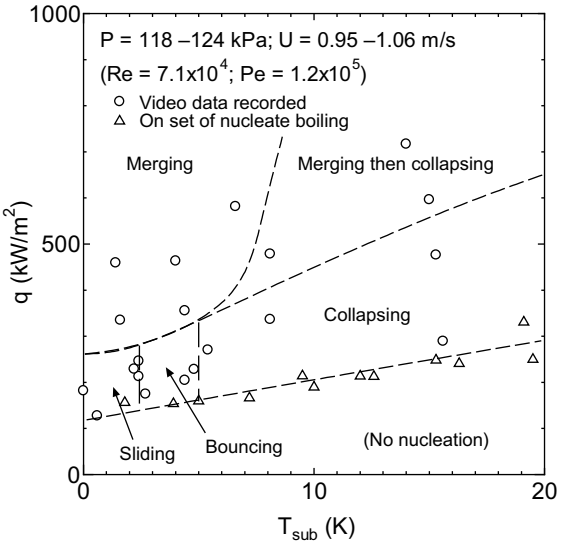

Fig. 5. Flow patterns observed in the test section tube.

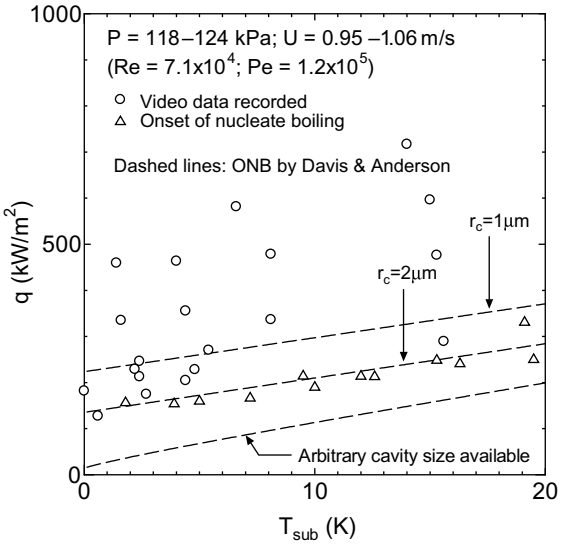

Fig. 6. Comparisons of the wall heat flux at the onset of nucleate boiling with the correlation by Davis and Anderson.

decreased and then collapsed due to the increased condensation rate even at the heat flux of 717 kW/m^2 (the region of merging then collapsing in Fig. 5).

If the bubble coalescence in the test section is not significant, the behavior of each bubble is observed clearly from the video data. In the present experiments, all the vapor bubbles departed from their nucleation sites immediately after the inception (bubbles moved upward from the nucleation sites already in the second images captured by high speed cameras); the following three typical bubble behaviors were observed after the departure from nucleation sites if the bubble did not merge with other bubbles:

(1) *Sliding bubble region at low subcooling:* The consecutive images of a typical sliding bubble are shown in Fig. 9. The sliding bubbles slid upward the vertical heated wall after the departure from a nucleation site and were not detached from the wall. Near the saturation temperature ($T_{sub} = 0.0$–0.6 K), all the bubbles were classified as the sliding bubble. In slightly subcooled water ($T_{sub} = 1.4$–2.7 K), approximately half of bubbles exhibited the sliding motion at lower heat flux ($q = 175$ kW/m^2) and the ratio of sliding bubbles increased up to approximately 80% at higher heat flux ($q = 246$ kW/m^2). The sliding bubbles were flattened along the wall at the inception but became more rounded gradually as they slid upward the vertical wall.

(2) *Bouncing bubble region at moderate subcooling:* The consecutive images of a typical bouncing bubble are shown in Fig. 10. The bouncing bubbles

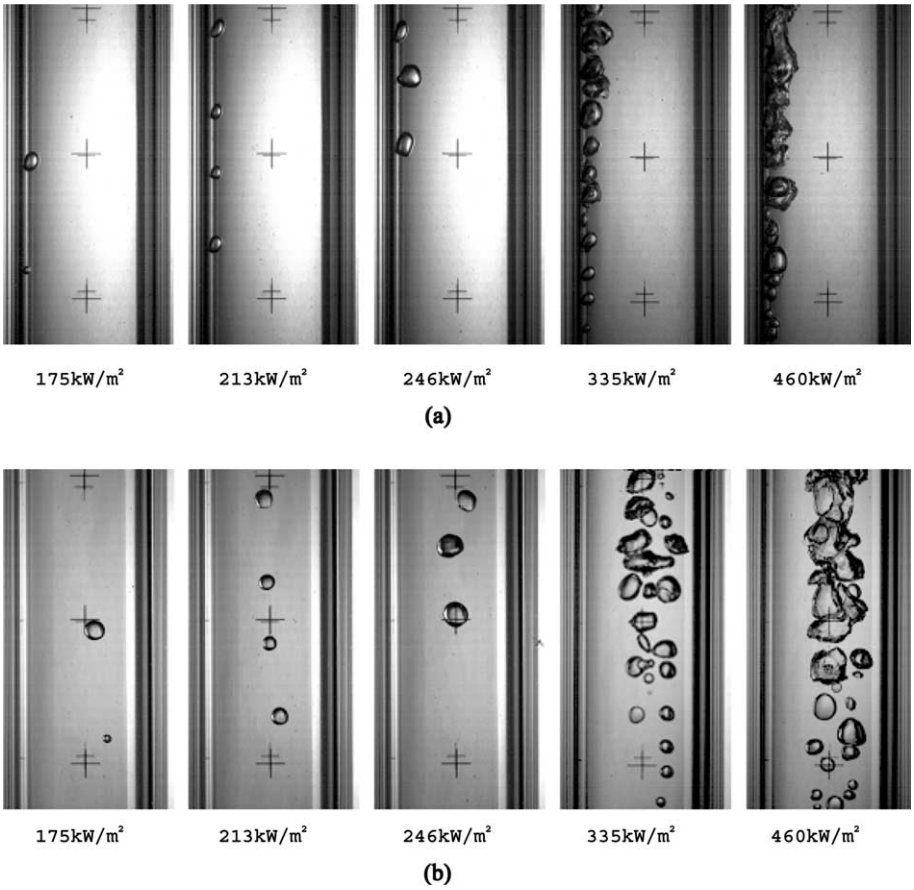

Fig. 7. Snapshots in the test section at low subcooling (cases B1–B6). (a) Side view and (b) bottom view.

were detached from the vertical heated surface after sliding upward the wall for several millimeters and then migrated towards the bulk liquid. The direction of lateral migration was then reversed to be reattached to the wall. After the reattachment, the bubbles exhibited the rebounding motion but the amplitude of detachment was much reduced. The bouncing bubbles were observed at moderate subcooling. In slightly subcooled water ($T_{sub} = 1.4$–2.7 K), both sliding and bouncing bubbles were observed; the ratio of bouncing bubbles decreased approximately from 50% to 20% as the heat flux was increased from 175 to 246 kW/m^2. When the subcooling was increased up to 4.4–5.4 K, approximately 80% of total bubbles were classified as the bouncing bubble at the heat flux of 205 kW/m^2; bouncing bubbles were also observed at higher heat fluxes but the ratio was indeterminate since multiple nucleation sites were activated.

(3) *Collapsing bubble region at high subcooling:* The consecutive images of a typical collapsing bubble are shown in Fig. 11. The behavior of collapsing bubbles after the departure from nucleation sites was almost the same as that of bouncing bubbles. However, they collapsed in the subcooled liquid after the detachment from the heated surface. Thus, they were not reattached to the wall. The bouncing bubbles also shrank after the detachment but they could be reattached to the wall before collapsing completely at lower liquid subcooling. At the liquid subcooling higher than 6 K, all the bubbles were classified as the collapsing bubble if they did not merge with other bubbles. At the lower subcooling of 4.4–5.4 K, rest of the bouncing bubbles also collapsed after the detachment from the wall to be classified as the collapsing bubbles.

It is known for adiabatic bubbly two-phase flow that many small bubbles are found adjacent to the tube wall if the flow direction is vertical upward [21]. This phenomenon is successfully described with the shear induced lift force that pushes the bubble towards the tube wall if the bubble rise velocity is higher than the

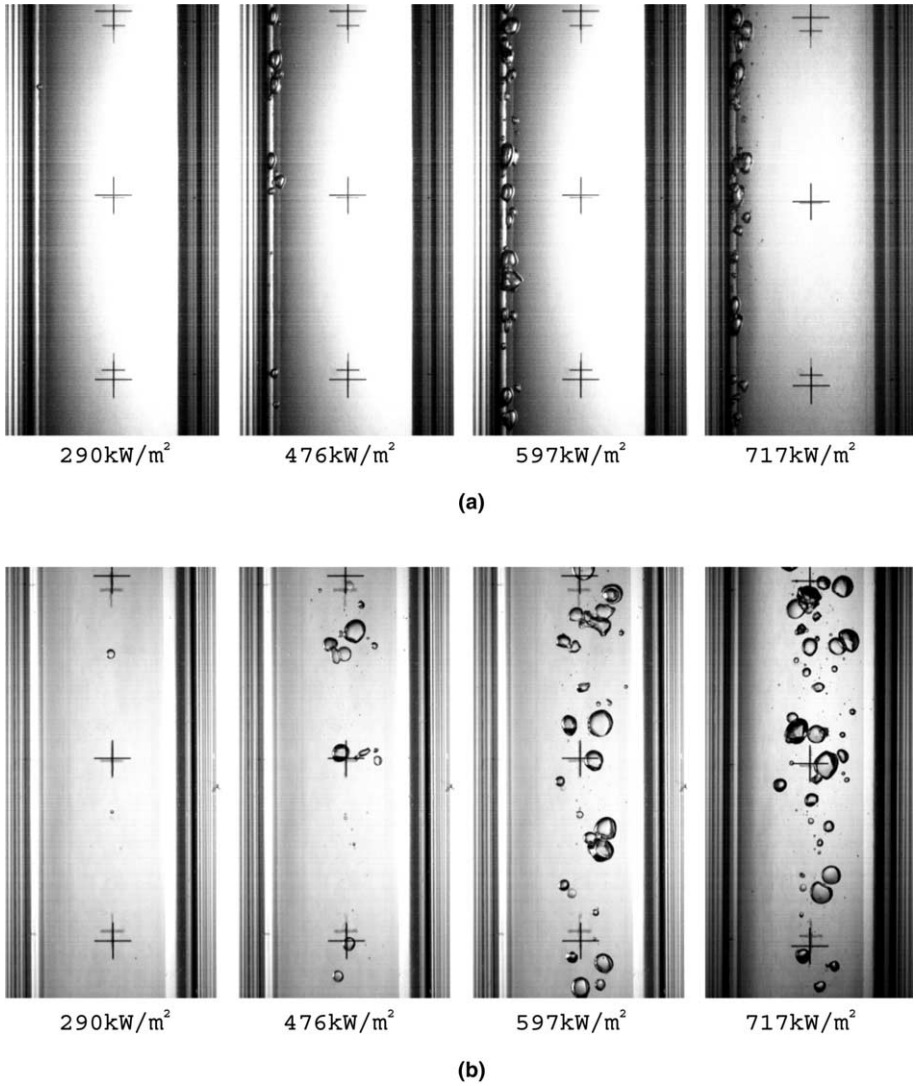

Fig. 8. Snapshots in the test section at high subcooling (cases E1–E4). (a) Side view and (b) bottom view.

local liquid velocity [22]. It is hence considered that, as partly discussed by Thorncroft et al. [17], the shear induced lift force is the primary cause of the sliding and the reattachment of bubbles observed in this work.

In the present experiments, bubbles experienced a short period of rapid growth after the inception and then the bubble size continued to increase or became fairly constant if the bubble was not detached from the wall. On the other hand, if the bubble was detached from the wall, the bubble size decreased due to the condensation and eventually collapsed at sufficiently high liquid subcooling. This indicates that understanding of bubble behavior after the departure from a nucleation site is of importance to elucidate the mechanisms of heat transfer and axial void growth in subcooled flow boiling.

3.3. Measurement of bubble dynamics

To obtain quantitative and more detailed information on the bubble rise characteristics, important bubble parameters are measured through image analysis. For consistency, image analyses are performed for the bubbles generated at the nucleation site A in Fig. 4. Bubble behavior is significantly influenced by other bubbles when many nucleation sites are activated. Thus, to elucidate the rise characteristics of single bubbles, the measurements are conducted for the video data obtained in the six experimental conditions (B1,

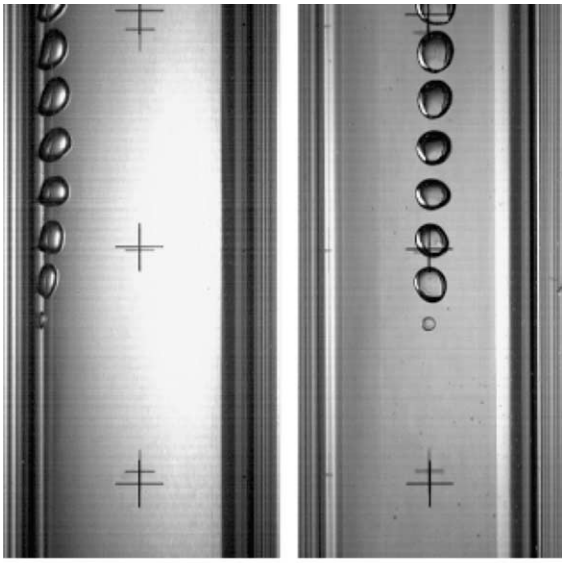

Fig. 9. Consecutive images of a typical sliding bubble (case B4; time interval is 4 ms). (a) Side view and (b) bottom view.

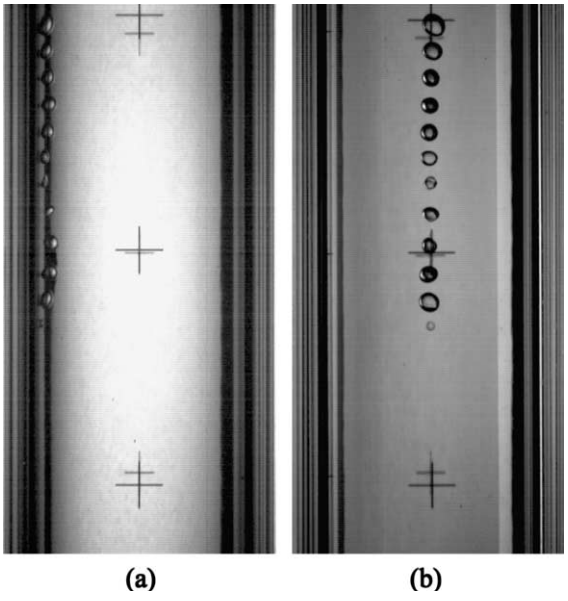

Fig. 10. Consecutive images of a typical bouncing bubble (case C1; time interval is 2.5 ms). (a) Side view and (b) bottom view.

B2, B4, C1, C2 and D1 in Table 1). The definitions of measured bubble parameters are shown schematically in Fig. 12. Because of the complicated deformation of bubbles observed in the experiments, the bubble size d_b is estimated by

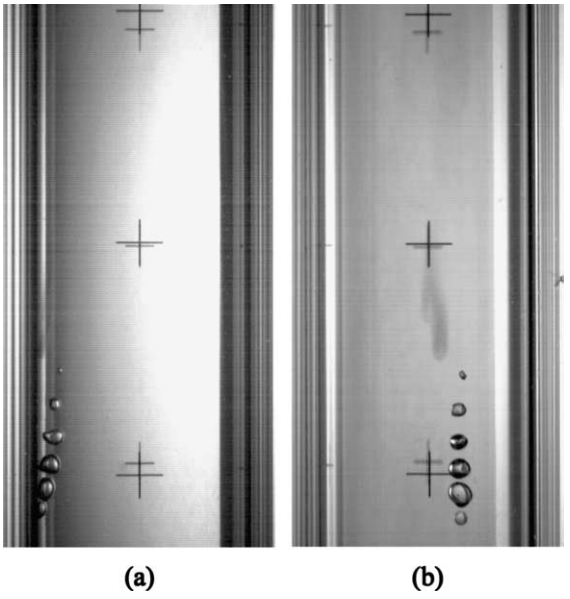

Fig. 11. Consecutive images of a typical collapsing bubble (case D1; time interval is 2.5 ms). (a) Side view and (b) bottom view.

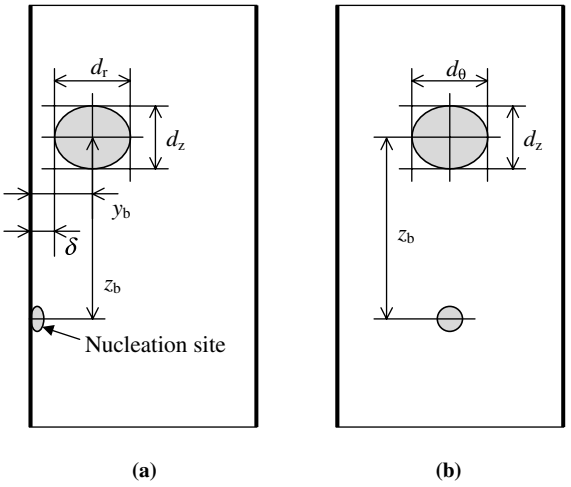

Fig. 12. Definitions of bubble parameters. (a) Side view and (b) bottom view.

$$d_b = \sqrt[3]{d_r d_z d_\theta} \tag{4}$$

where d_r, d_z and d_θ denote the maximum dimensions of a bubble in the radial, axial and circumferential directions, respectively. To denote the deformation level, the modified aspect ratio R_A is defined by

$$R_A = \frac{d_r}{d_b} \tag{5}$$

It is recognized from Fig. 12 that $R_A = 1$ if the bubble is spherical, $R_A < 1$ if the bubble is flattened along

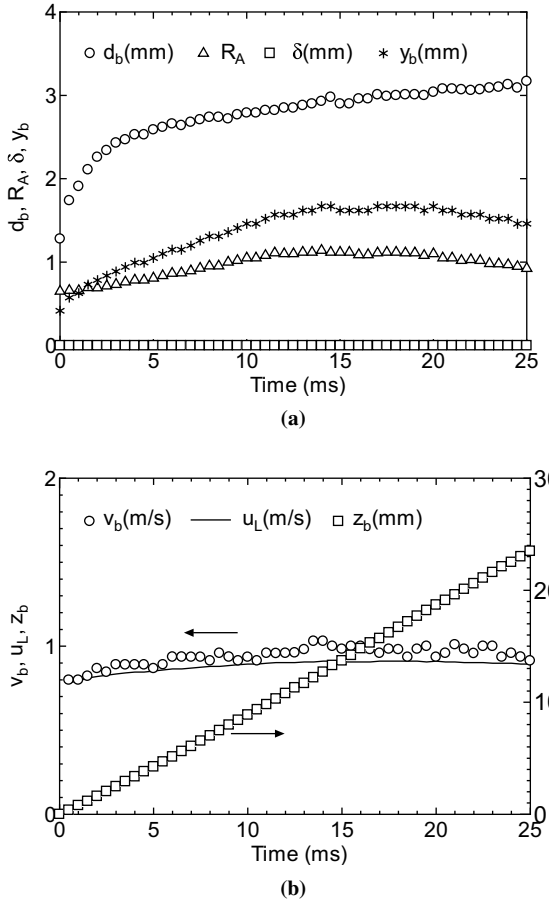

Fig. 13. Time series of bubble parameters for a sliding bubble (case B1). (a) Size, shape, and lateral position and (b) rise velocity and vertical position.

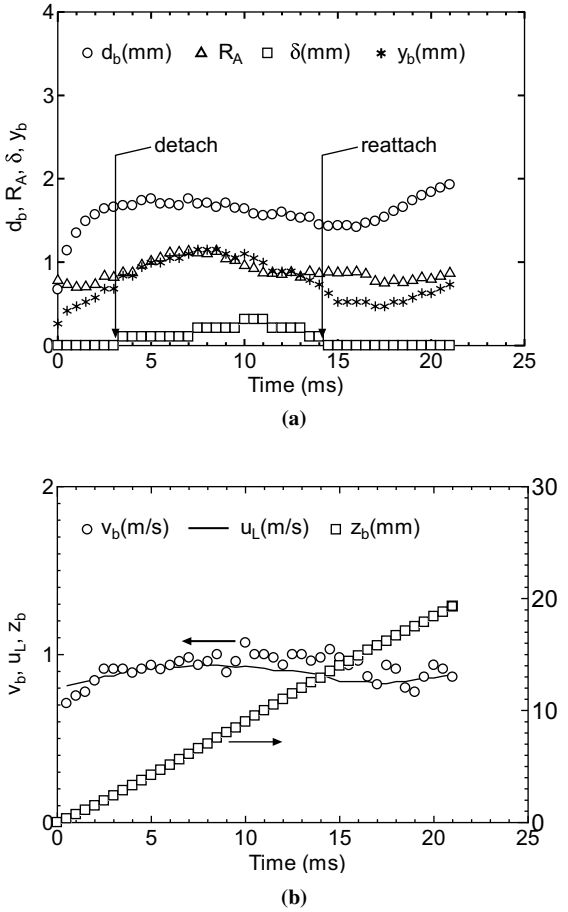

Fig. 14. Time series of bubble parameters for a bouncing bubble (case C1). (a) Size, shape, and lateral position and (b) rise velocity and vertical position.

the wall and $R_A > 1$ if the bubble is elongated in the lateral direction.

The results of image analysis for a typical sliding bubble are shown in Fig. 13. At the instant of inception at a nucleation site, the bubble is flattened along the wall ($R_A = 0.65$). The bubble experiences rapid growth for a few milliseconds and then the growth rate is reduced. Fig. 13(b) indicates that the bubble starts sliding along the wall immediately after the inception at a nucleation site and the rise velocity v_b becomes comparable with u_l within 1 ms. Here, the local liquid velocity at the bubble center position u_l is estimated from Nunner's expression [19]. The bubble shape becomes more rounded and R_A reaches unity at approximately 10 ms after the nucleation.

The results for typical bouncing and collapsing bubbles are shown in Figs. 14 and 15, respectively. These bubbles are also flattened along the wall at the inception ($R_A < 1$). For a short period of time after the inception, R_A is fairly constant or slightly decreasing. This may be attributed to the rapid growth in bubble size. When the rapid growth in the initial stage is ceased, the bubbles become more rounded. Shorter period of time (approximately 5 ms) is sufficient for R_A to be unity. The surface tension force would be the primary reason for the shape change from flattened to more rounded. Since the influence of surface tension force is more prominent for smaller bubbles, the rapid change in bubble shape could be attributed to the smaller growth rate of these bubbles. In fact, as partly indicated in Figs. 13–15, the bouncing and collapsing bubbles were generally smaller than the sliding bubbles. For a short period of time after the inception, the increase in d_b leads to the increase in y_b (y_b is the distance between bubble center and wall). Though the rapid increase in d_b is ceased within a few milliseconds, y_b continues to increase due to the change in bubble shape (note that the increase of R_A results in the increase of y_b if the bubble is attached to the wall and bubble size is constant). Since y_b is kept increasing

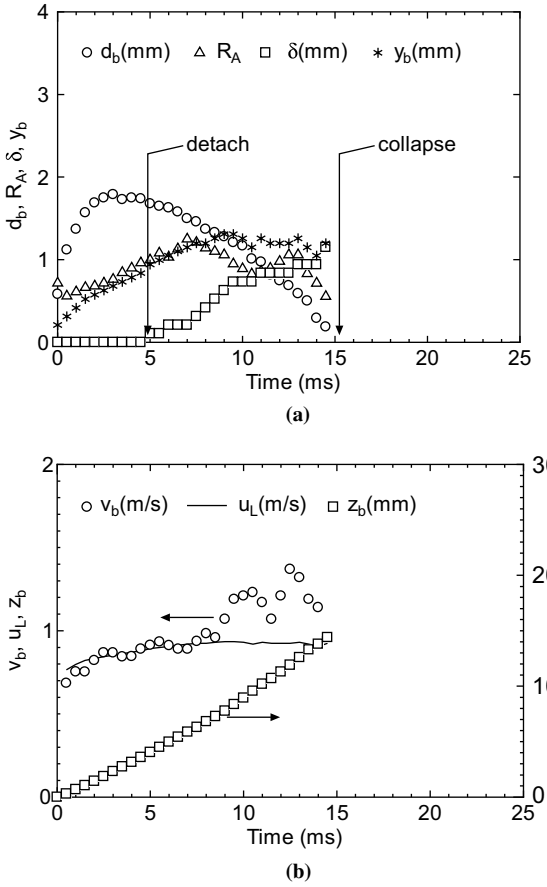

Fig. 15. Time series of bubble parameters for a collapsing bubble (case D1). (a) Size, shape, and lateral position and (b) rise velocity and vertical position.

after d_b becomes fairly constant, the bubbles are eventually detached from the wall ($\delta > 0$).

Illustrated in Fig. 16 is the supposed mechanism for the detachment of a bubble from a vertical heated wall. If the bubble shape is changed from flattened to more rounded, liquid flow directed toward the bottom of a bubble may be formed. The inertia of this liquid flow can be the driving force to lift the bubble from the vertical wall. It is hence considered that the initial bubble shape flattened along the wall and the following change to more rounded shape is the main cause for the bubble detachment. After the detachment, the bouncing bubble and collapsing bubble behave differently. Fig. 14 indicates that the bouncing bubble stays near the wall after the detachment to be reattached to the wall. The occurrence of reattachment may be attributed to the shear induced lift force. The bubble size d_b decreases gradually after the detachment due to the condensation in subcooled bulk liquid but increases after the reattachment. Some bubbles are detached again after the reattachment

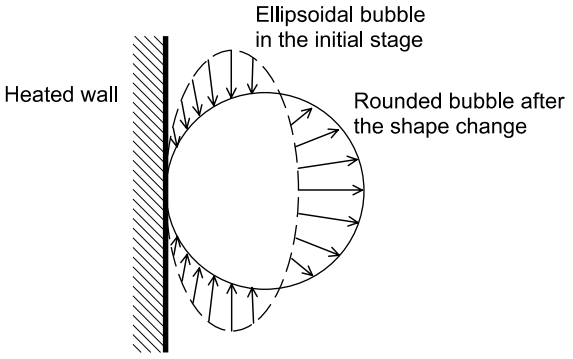

Fig. 16. Supposed flow field around the bubble during shape change.

though the amplitude is much reduced. As shown in Fig. 15, a bubble is collapsed after the detachment if the subcooling of bulk liquid is sufficiently high. The bubble is suddenly accelerated while it is shrinking. This may indicate that the condensation is more prominent at the rear of the bubble.

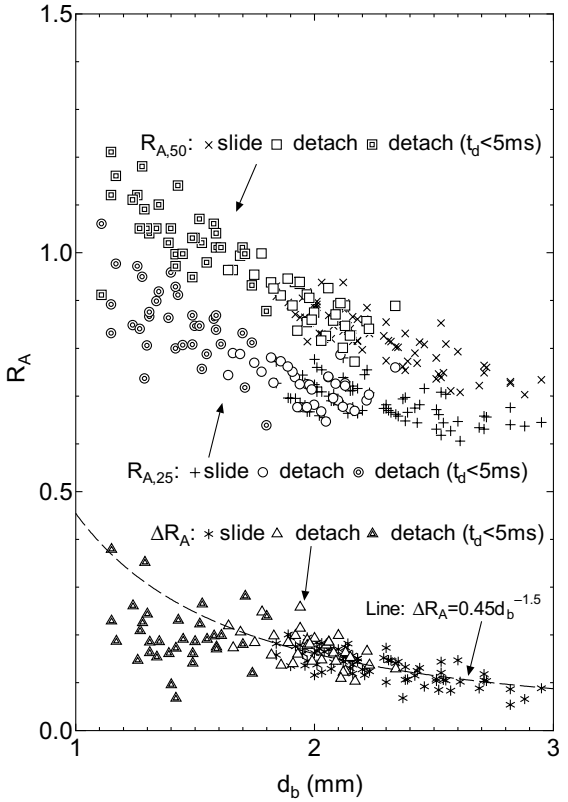

Fig. 17. Relation between d_b and R_A within the initial stage after the inception.

The effect of surface tension would be more prominent for smaller bubbles. It is hence inferred from the above investigation that larger driving force for the detachment is provided if the growth rate within a short period after the inception is smaller. In view of this, the aspect ratios at 2.5 and 5.0 ms after the inception $R_{A,25}$ and $R_{A,50}$ are plotted against the bubble size d_b in Fig. 17, where d_b is evaluated by $d_b = (d_{b,25} + d_{b,50})/2$. Though there exists scattering, it is confirmed that sliding bubbles experience faster growth than detached bubbles (bouncing and collapsed bubbles) during the initial stage and consequently d_b is approximately greater than 2 mm. Smaller R_A for sliding bubbles indicates the slower shape change due to the smaller surface tension force. In Fig. 17, the difference in the aspect ratios at two time levels $\Delta R_A = R_{A,25} - R_{A,50}$ is also plotted against d_b. As denoted with the dashed line, ΔR_A is approximately proportional to $d_b^{-1.5}$ if a bubble is still attached to the wall at 5 ms after the inception. This fact may support that the surface tension force is the primary cause of the shape change observed, since it is known analytically that the frequency is proportional to $d_b^{1.5}$ for the small oscillation of a gas bubble about the spherical form in an infinite stagnant liquid [24].

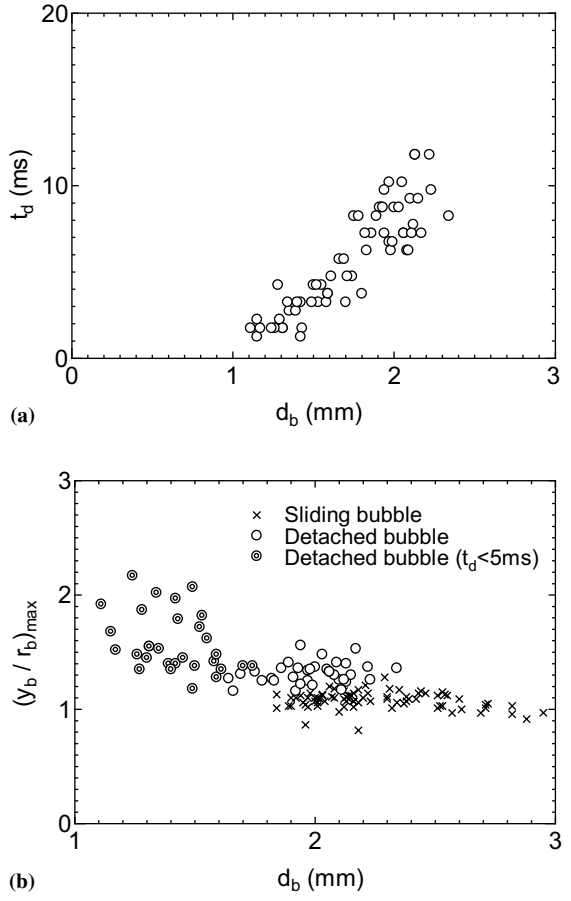

Fig. 18. Influence of initial bubble growth rate on the bubble rise characteristics. (a) Influence on the detachment time and (b) influence on the normalized maximum distance from wall.

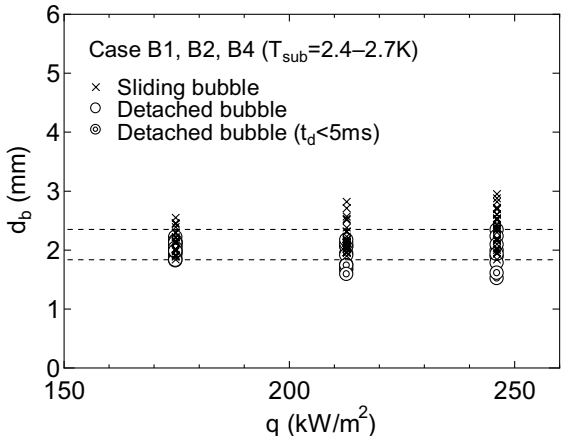

Fig. 19. Influence of heat flux on the bubble rise path.

Fig. 18(a) and (b) show the effects of d_b on the time for the onset of detachment t_d and the normalized maximum distance between bubble center and wall $(y_b/r_b)_{max}$, respectively. The results are plotted only for detached bubbles in Fig. 18(a) since t_d is indeterminate for sliding bubbles while plotted for all the bubbles in Fig. 18(b). The figures indicate that the decrease in d_b results in the decrease of t_d and the increase of $(y_b/r_b)_{max}$. It can hence be said that the bubble rise path after the departure from a nucleation site is significantly influenced by the growth rate of a bubble during the short period after the inception. It is inferred that evaporation beneath a bubble retards the bubble detachment since the phase interface approaches to the wall. The values of d_b for sliding and bouncing bubbles in the cases B1, B2 and B4 are plotted against q in Fig. 19. Liquid subcooling is within 2.4–2.7 K in these three cases. The ratio of sliding bubbles increases with q. However, the boundary between the sliding and detached bubbles can be determined by d_b and the critical bubble size is not influenced significantly by q within the heat flux range tested. It is hence considered that the ratio of sliding bubbles increased with q because of the increase in growth rate during the initial stage after the inception.

4. Summary and conclusions

A visual experimental study was performed to elucidate the bubble behavior in subcooled upflow boiling

of water. The test section was a sapphire glass tube of 20 mm in inside diameter; pressure and volumetric flux were kept around 120 kPa and 1 m/s, respectively, while liquid subcooling was varied within 0–16 K. Two high speed video cameras were used to observe the behavior of single vapor bubbles that were generated at their nucleation sites on the inner surface of glass tube. Detailed image analyses were conducted to measure important bubble parameters. Since the video data in which a small number of nucleation sites were activated were used in the image analyses, significant influence from neighboring bubbles would be avoided. The main observations of the present experiments are summarized as follows:

(1) In the present experimental conditions, almost all the bubbles departed from their nucleation sites within 1 ms after the inception. From the rise paths after the departure from the nucleation site, the bubbles were classified into three categories: sliding, bouncing and collapsing bubbles. The sliding bubbles slid upward the vertical heated surface after the departure from nucleation sites and consequently were not detached from the wall. On the other hand, the bouncing and collapsing bubbles were detached from the wall after sliding along the wall for several millimeters. The bouncing bubbles then reversed the direction of lateral migration and were reattached to the wall. These bubbles exhibited rebounding motion after the reattachment. Some bubbles were detached from the wall again but the amplitudes were much reduced. The collapsing bubbles disappeared due to the condensation after the detachment from the heated wall; thus, they were not reattached to the wall.

(2) The bubbles were flattened along the vertical wall at the inception at their nucleation sites and then became more rounded due to the surface tension force. If the bubble varies from flattened to more rounded shape, the liquid flow directing toward the bottom of bubble would be formed. The inertia of liquid flow beneath the bubble was considered the main driving force to detach the bubble from the wall. The sliding bubbles were generally larger than the bouncing and collapsing bubbles since they experienced more rapid growth during the initial stage after the inception. The larger bubble size resulted in slower shape change due to the reduced surface tension force. This was estimated as the primary reason for the sliding bubbles not to be detached from the vertical wall. The growth rate of a bubble during the initial stage was reduced with the increase of subcooling. Thus, the ratio of sliding bubbles to all the bubbles generated was also reduced with the increase of subcooling. The collapsing bubbles were observed more frequently at higher liquid subcooling due to increased condensation rate.

(3) The number of activated nucleation sites was increased with the heat flux applied to the test section. Since some newly activated nucleation sites generated larger bubbles with lower frequency and bubbles generated at different nucleation sites were merged, the size of largest bubble in the test section was increased with heat flux. In low subcooling experiments, the sizes of large bubbles were not reduced since they repeated the coalescence with other bubbles. In high subcooling experiments, bubbles were frequently merged but they were collapsed due to the condensation within the heat flux range tested.

References

[1] S. Levy, Forced convection subcooled boiling prediction of vapor volumetric fraction, Int. J. Heat Mass Transfer 10 (1967) 951–965.
[2] P. Saha, N. Zuber, Point of net vapor generation and vapor void fraction in subcooled boiling, in: Proceedings of 5th International Heat Transfer Conference, 1974, pp. 175–179.
[3] P.G. Kroeger, N. Zuber, An analysis of the effects of various parameters on the average void fractions in subcooled boiling, Int. J. Heat Mass Transfer 11 (1968) 211–233.
[4] H. Lin-wen, P. Chin, Predictions of void fraction in convective subcooled boiling channels using a one-dimensional two-fluid mode, Trans. ASME, J. Heat Transfer 117 (1995) 799–803.
[5] H.O. Chang, J.C. Chapman, Two-phase flow instability for low-flow boiling in vertical heated thin rectangular channels, Nucl. Technol. 113 (1996) 327–337.
[6] F.C. Gunther, Photographic study of surface-boiling heat transfer to water with forced convection, Trans. ASME 73 (1951) 115–123.
[7] L.M. Jiji, L.A. Clark, Bubble boundary layer and temperature profiles for forced convection boiling channel flow, Trans. ASME, J. Heat Transfer 86 (1964) 50–58.
[8] W. Frost, C.J. Kippenhan, Bubble growth and heat transfer mechanisms in the forced convection boiling of water containing a surface active agent, Int. J. Heat Mass Transfer 10 (1967) 931–949.
[9] A.H. Abdelmessih, F.C. Hooper, S. Nangia, Flow effects on bubble growth and collapse in surface boiling, Int. J. Heat Mass Transfer 15 (1972) 115–125.
[10] M. Akiyama, F. Tachibana, Motion of vapor bubbles in subcooled heated channel, Bull. JSME 17 (1974) 241–247.
[11] V.H. del Valle, D.B.R. Kenning, Subcooled flow boiling at high heat flux, Int. J. Heat Mass Transfer 28 (1985) 1907–1920.
[12] E.L. Bibeau, M. Salcudean, A study of bubble ebullition in forced-convective subcooled nucleate boiling at low pressure, Int. J. Heat Mass Transfer 37 (1994) 2245–2259.
[13] O. Zeitoun, M. Shoukri, Bubble behavior and mean diameter in subcooled flow boiling, Trans. ASME, J. Heat Transfer 118 (1996) 110–116.
[14] V. Prodanovic, D. Fraser, M. Salcudean, Bubble behavior in subcooled flow boiling of water at low pressures and low flow rates, Int. J. Multiphase Flow 28 (2002) 1–19.

[15] M.G. Cooper, K. Mori, C.R. Stone, Behaviour of vapor bubbles growing at a wall with forced flow, Int. J. Heat Mass Transfer 26 (1983) 1489–1507.
[16] W.G.J. van Helden, C.W.M. van der Geld, P.G.M. Boot, Forces on bubbles growing and detaching in flow along a vertical wall, Int. J. Heat Mass Transfer 38 (1995) 2075–2088.
[17] G.E. Thorncroft, J.F. Klausner, R. Mei, An experimental investigation of bubble growth and detachment in vertical upflow and downflow boiling, Int. J. Heat Mass Transfer 41 (1998) 3857–3871.
[18] T. Okawa, T. Ishida, I. Kataoka, M. Mori, An experimental study on bubble rise path after the departure from a nucleation site in vertical upflow boiling, Exp. Therm. Fluid Sci. 29 (2005) 287–294.
[19] J.O. Hinze, Turbulence, McGraw-Hill, New York, 1959 (Chapter 7).
[20] E.J. Davis, G.H. Anderson, The incipience of nucleate boiling in forced convective flow, AIChE J. 12 (1966) 774–780.
[21] A. Serizawa, I. Kataoka, I. Michiyoshi, Phase distribution in bubbly flow, in: G.F. Hewitt et al. (Eds.), Multiphase Science and Technology, vol. 6, Hemisphere, New York, 1992, pp. 257–301.
[22] T. Okawa, I. Kataoka, M. Mori, Numerical simulation of lateral phase distribution in turbulent upward bubbly two-phase flows, Nucl. Eng. Des. 213 (2002) 183–197.
[23] W.-C. von Ceumern-Lindenstjerna, Bubble departure and release frequencies during nucleate pool boiling of water and aqueous sodium chloride solutions, in: E. Hahne, U. Grigull (Eds.), Heat Transfer in Boiling, Hemisphere, New York, 1977 (Chapter 3).
[24] H. Lamb, Hydrodynamics, sixth ed., Cambridge University Press, Cambridge, 1932 (Chapter 9).